

Directional Coupling of Emitters into Waveguides: A Symmetry Perspective

Aristeidis G. Lamprianidis,* Xavier Zambrana-Puyalto, Carsten Rockstuhl, and Ivan Fernandez-Corbaton*

Recent experiments demonstrate strongly directional coupling of light into waveguide modes. Here, the symmetry mechanisms behind this effect are studied, and it is shown that the analysis of the symmetries and symmetry-breakings of the emitter-waveguide system allows to qualitatively understand directional coupling in several situations. The authors consider emitters either centered in a median plane of the waveguide, or displaced from it, and whose emissions have a well-defined angular momentum in either one of the two different axis typically chosen experimentally, which are called transverse and vertical. These insights are matched by simulations, and previous experimental measurements. It is shown that handedness plays a secondary role in directional coupling. The spin-momentum locking concept is generalized to an exponentially strong locking between the transverse angular momentum and the preferential coupling direction. A new selection rule is obtained that controls the coupling of electric(magnetic) multipolar emissions into waveguide modes. An experiment is proposed featuring a transverse magnetic bias that aggregates the directional emissions from many quantum dots on top of waveguides, in contrast to the typically used vertical bias, which effectively restricts experiments to using a single quantum dot. Finally, the Huygens' dipole is analyzed and the symmetries that enable its directional behavior revealed.

1. Introduction and Summary

Several recent experiments have demonstrated directional coupling of light into waveguide modes. For example, pronounced directionality has been shown in the collection of atomic emissions by optical fibers^[1] and quantum dot emissions by waveguides.^[2–5] Similarly, experiments have shown pronounced directional coupling of focused light beams into waveguides, either directly,^[6] or mediated by a scatterer.^[7,8] The directionality effect has the potential to route light and classify emissions according to the electromagnetic properties that determine the preferential coupling direction.


Different theoretical approaches have been developed to understand the effect.^[9–22] In particular, the concepts of transverse spin and spin-momentum locking in evanescent waves have been put forward as the origin of the directionality. Yet, there are some open questions. The use of the photonic spin introduces an ambiguity: In the context of the common separation of the optical

angular momentum into orbital and spin parts,^[23,24] the spin of the photon is often simultaneously connected to both angular momentum and circular-polarization handedness (e.g., refs. [13,25–27]). This raises the question of which property dictates the directional coupling. Each of the two options implies fundamentally different characteristics and applications of the directional coupling effect. Also, a static magnetic field or the incident excitation is used in experiments to choose the axis of well-defined angular momentum for the emissions. One of two different options, which we call transverse axis,^[1,7,8] and vertical axis,^[2–5,12] is typically selected. The concept of spin-momentum locking only applies naturally to the transverse case. More generally, the dipolar approximation is routinely made to characterize the emitter. This precludes the theoretical study and prediction of possible directional coupling effects for the light emitted from higher-order multipolar transitions of atoms, molecules, and quantum dots.^[28–33] Finally, while the numerical evaluation of the directionality in particular systems is, at least for dipolar emitters, relatively straightforward,^[1–5,7,8,12,34] it is often unclear as to how to use the results for extracting general insights that would apply to more general situations.

A. G. Lamprianidis, C. Rockstuhl
Institute of Theoretical Solid State Physics
Karlsruhe Institute of Technology
76128 Karlsruhe Germany
E-mail: aristeidis.lamprianidis@kit.edu

C. Rockstuhl, I. Fernandez-Corbaton
Institute of Nanotechnology
Karlsruhe Institute of Technology
76021 Karlsruhe Germany
E-mail: ivan.fernandez-corbaton@kit.edu

X. Zambrana-Puyalto
Istituto Italiano di Tecnologia
Via Morego 30, 16163 Genova Italy

 The ORCID identification number(s) for the author(s) of this article can be found under <https://doi.org/10.1002/lpor.202000516>

© 2021 The Authors. Laser & Photonics Reviews published by Wiley-VCH GmbH. This is an open access article under the terms of the Creative Commons Attribution-NonCommercial-NoDerivs License, which permits use and distribution in any medium, provided the original work is properly cited, the use is non-commercial and no modifications or adaptations are made.

DOI: 10.1002/lpor.202000516

In this work, we use a symmetry-based approach to study the directional coupling effect. One advantage of symmetry arguments is their general applicability. As long as the insights about an effect in a particular system are obtained only by symmetry arguments, they will apply generally to other systems with the same symmetries. In particular, the trends and qualitative results that we present are independent of the waveguide materials and of whether the waveguide is single-mode or multi-mode, as long as the emitter-plus-wave-guiding system meets the symmetry requirements that we identify.

In our approach, we will not separate the generator of rotations, that is, the angular momentum into orbital and spin parts.^[14,35] This avoids the possible confusion between the spin part and the helicity(handedness) of light, and allows us to separately study the roles that the helicity and the angular momentum of the emissions play in the directional coupling. This approach has already been proven successful in predicting some different effects that the two properties can have in light–matter interactions.^[36–38]

The outline of the article is as follows. Section 2 contains numerical simulations of the coupling of single multipolar emissions near a rectangular waveguide. The emissions are single multipoles with well-defined transverse angular momentum and helicity, and are centered in a median plane of the waveguide. The simulations show that the magnitude of the directionality grows roughly exponentially with the absolute value of the transverse angular momentum. We analytically show in Section V, Supporting Information, that the exponential growth is due to an intrinsic characteristic of the evanescent components of the emissions, whose power flux in the relevant directions depends exponentially on the transverse angular momentum. A similar exponential growth is observed, for most cases, in the coupling efficiency, which is defined here as the power coupled into the waveguide divided by the power that the emitter would radiate to the far field in the absence of the waveguide. The results in Section 2 also contain several regularities that hint toward the existence of general rules, which we obtain by symmetry analysis in Section 3.1: The directionality is due to the breaking of a particular mirror symmetry due to the axial character of the angular momentum vector; the sign of the transverse angular momentum vector determines the preferred coupling direction; for emitters centered in the median plane, the helicity of the emission has no effect in the directionality. We then hypothesize and confirm with extra simulations that the correlation between the preferred coupling direction and the sign of the angular momentum does not depend on the displacement of the emitter from the median plane, and that the helicity of a displaced emitter can have some effect on the directionality, which, in the simulations, is seen to be rather small with respect to the dominant angular momentum contribution.

Several of the results for helical emissions apply to the more common electric and magnetic multipolar emissions as well. There is, however, one important difference: An electric(magnetic) multipolar emission will feature a directionality identical to that of the corresponding helical emissions, implying the exponential scaling of the directionality with the magnitude of the transverse angular momentum, provided that the electric(magnetic) emission couples to the waveguide mode. This is a difference with respect to the helical emissions: We deduce

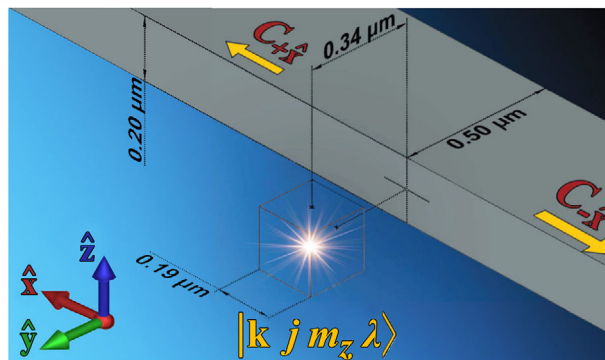


Figure 1. Sketch of the geometry of the system representing the coupling of the multipolar emission $|k j m_z \lambda\rangle$ to a nearby silicon waveguide of refractive index equal to 3.478. The emitter is located in vacuum at the center of the coordinate system. The waveguide is placed symmetrically with respect to the xOy plane with its optical axis parallel to the x -axis. The radiated power that couples to the first guided mode of the waveguide toward either the $+x$ or the $-x$ directions is collected by waveguide ports.

a new selection rule for a centered electric(magnetic) multipolar emission, which must be met for it to couple to a given waveguide mode. We have confirmed the selection rule by simulations (not included here). Such selection rule does not apply to helical emissions.

Section 3.2 is devoted to the symmetry analysis of the directionality of emissions with well-defined vertical angular momentum, independently of their helical or electric/magnetic character. We find, in agreement with published experimental results like, for example, ref. [5], that the preferred coupling direction for a given sign of the angular momentum depends on the sign of the displacement of the emitter, and that it is zero for emitters centered in a waveguide that is invariant under reflections across this median plane. In Section 3.3, we then propose an experiment where the emissions from many quantum dots on top of waveguides would aggregate in a directionality preserving way. This is a yet unobserved effect that overcomes the current effective restriction to collecting the signal from a single quantum dot.

In Section 3.4, we analyze the Huygens' dipole, which contains different angular momentum components. We reveal the origin of its directionality by showing that the Huygens' dipole breaks and maintains the same relevant symmetries as a single electric(magnetic) multipolar emission with well-defined transverse angular momentum. The same symmetry situation is achieved by means of two different properties: the axial character of the transverse angular momentum on the one hand, and a particular combination of electric and magnetic dipoles in the Huygens dipole on the other.

Section 4 contains the final remarks, where, in particular, we highlight the advantages of higher order emissions in terms of both directionality and coupling efficiency, and the fact that the directional coupling effect, being mostly independent of the helicity of the emissions, cannot be used for the efficient sensing of chiral molecules.

Before starting, the definition of the transverse and vertical axis is in order. The vertical axis is perpendicular to the waveguide axis, and lies on a median plane of the waveguide which contains the waveguide axis. In **Figure 1**, the y axis is the vertical axis. The

transverse axis is also perpendicular to the waveguide axis, does not intersect with the waveguide, and the plane perpendicular to it is a median plane of the waveguide. In Figure 1, the \mathbf{z} axis is the transverse axis. Experimentally, a static magnetic bias or the optical axis of the illumination is used to choose one of the two axis.

2. Numerical Simulations

We start analyzing the transverse case by means of numerical simulations of the directionality of single multipolar emissions with well-defined transverse angular momentum. This axis has been selected in several directional coupling experiments like, for example, ref. [1, 7, 8]. In the simulations that we present in this section, each emission contains a single helical multipole. The salient characteristic of the helical multipoles is that all the plane-waves in their decomposition, including the evanescent ones, have the same polarization handedness. The choice of helical emissions allows to us to study the separate effect that angular momentum and handedness (helicity),^[39–42] that is, the rotational or chiral properties of the emissions, may have on the directional coupling effect. We denote the helical multipoles by $|kj m_z \lambda\rangle$, where k is the wavenumber, j is the multipolar order (dipole $j = 1$, quadrupole $j = 2$, etc ...), $m_z \in [-j, -j + 1, \dots, j - 1, j]$ is the projection of angular momentum along the z axis, and $\lambda \in \{-1, +1\}$ is the helicity (handedness). The helical multipoles, or multipoles of well-defined helicity are linear combinations of the electric and magnetic multipoles (see ref. [43], Eq. (11.4–25), and ref. [44], Eq. (2.18)). The multipoles of well-defined helicity $|kj m_z \lambda\rangle$ can be written as the following linear combinations of the electric and magnetic multipoles $|kj m_z \tau\rangle$:

$$|kj m_z \lambda\rangle = \frac{|kj m_z \tau = -1\rangle + \lambda |kj m_z \tau = +1\rangle}{\sqrt{2}} \quad (1)$$

where $\tau = 1 (\tau = -1)$ corresponds to the electric (magnetic) multipoles. Section I, Supporting Information, contains the conventions that we use in this article and explicit expressions and relevant symmetry properties of helical multipoles. Any emission can be decomposed into helical multipoles. They form a complete basis for the fields radiated by an arbitrary emitter. For example, the fields emitted by an arbitrarily-oriented electric dipole \mathbf{p} of frequency $\omega = kc_0$ can be written as (see Section II, Supporting Information):

$$\sum_{m_z=-1}^{m_z=1} p_{m_z} (|k 1 m_z +\rangle - |k 1 m_z -\rangle) \quad (2)$$

where the weights p_{m_z} are proportional to the projection of the spherical basis vectors $\{\hat{\mathbf{e}}_{-1} = (\mathbf{x} - i\mathbf{y})/\sqrt{2}, \hat{\mathbf{e}}_0 = \mathbf{z}, \hat{\mathbf{e}}_1 = -(\mathbf{x} + i\mathbf{y})/\sqrt{2}\}$ onto \mathbf{p} . We note that angular momentum and helicity can be most easily confused in the dipolar approximation. The field radiated by what is commonly referred to as [2, 3, 5, 12, 18] circular-dipole or circularly polarized electric dipole moment $\mathbf{p} = -\mathbf{x} - i\mathbf{y}$ ($\mathbf{p} = \mathbf{x} - i\mathbf{y}$), has a single non-zero coefficient p_1 (p_{-1}) in Equation (2). The radiation of a circularly polarized electric dipole has hence a well-defined angular momentum $m_z = 1$ or

$m_z = -1$, but is a perfect mix of the two helicities. When our results are particularized to the dipolar approximation, it is seen that the preferred coupling direction is determined by the \pm sign in $\mathbf{p} = \pm\mathbf{x} - i\mathbf{y}$ because such sign determines the transverse angular momentum $m_z = \mp 1$ of the radiated fields, not because it reflects the helicity of the emitted light. Crucially, while such \pm sign is reminiscent of a binary property like chirality or handedness, it should not be identified with it. For one thing, such identification leaves the $m_z = 0$ dipolar emission out of the framework. Moreover, such incorrect identification consequently implies that the directional effect is always binary, while, as we show later, it rather features an m_z -dependent non-binary gradation.

Figure 1 shows the considered geometry. An emitter is placed at the origin of the coordinate system close to a nearby rectangular silicon waveguide. The refractive index of silicon is assumed to be equal to 3.478. The waveguide is invariant under reflections across the xOy and yOz planes, and is parallel to the x -axis. The distance between the emitter and the axis of the waveguide is 590 nm. The width of the waveguide is 500 nm and its height is 200 nm. We perform numerical simulations over a frequency window of 40 THz centered at $f_0 \approx 193.4$ THz. The central frequency corresponds to a vacuum wavelength of 1550 nm, and the frequency span to a wavelength range between 1404 and 1729 nm. For practical purposes, the waveguide can be considered single-mode across the entire frequency band. The simulations are performed in the time domain using CST MWS. Section III, Supporting Information, contains detailed explanations. We consider emissions up to the octupolar order ($j = 3$) for both helicities and all possible values of m_z , for a total of $30 = (3+5+7) \times 2$ cases. The directionality is computed as follows. After the emission, a portion of the radiated power couples into the waveguide. The power coupled to the first waveguide mode travelling toward either the $+\hat{x}$ or the $-\hat{x}$ direction is recorded by two dedicated ports. We refer to the power coupled toward the $\pm\hat{x}$ direction as $C_{\pm\hat{x}}$. Figure 2 shows the logarithmic directionality of the in-coupled power $D = \log_{10}[C_{+\hat{x}}/C_{-\hat{x}}]$ for varying transverse angular momentum m_z , multipolar order j , and helicity λ . A positive (negative) D indicates preferential coupling toward the $+\hat{x}$ ($-\hat{x}$) direction, and $|D|$ measures the degree of directionality in a logarithmic scale. For each (m_z, j) , the data in blue (red) corresponds to the positive (negative) helicity. The color intensity encodes the histogram of D as indicated by the insets. Each histogram is the distribution of the directionality obtained from a wideband numerical simulation. A more (less) intense color corresponds to a more (less) frequent occurrence of a particular directionality value in the simulation results. On the one hand, Figure 2 clearly shows that the helicity does not influence the value of D : Emissions with the same multipolar content (m_z, j) but opposite helicity produce the same values of D .^[45] We will later show that this follows from the symmetries of the system. On the other hand, Figure 2 shows a clear dependence of D on the transverse angular momentum m_z , which approximately follows^[46] the green dashed line corresponding to $2m_z$. The sign of m_z fixes the preferential coupling direction and in a linear scale, the degree of directionality grows approximately as $10^{2|m_z|}$. We also observe that two emissions a and b, with $(m_z, j)_a$ and $(-m_z, j)_b$ result in $D_a = -D_b$, and that for $m_z = 0$, $D \approx 0$. These regularities will be also shown to follow from the symmetries of the system.

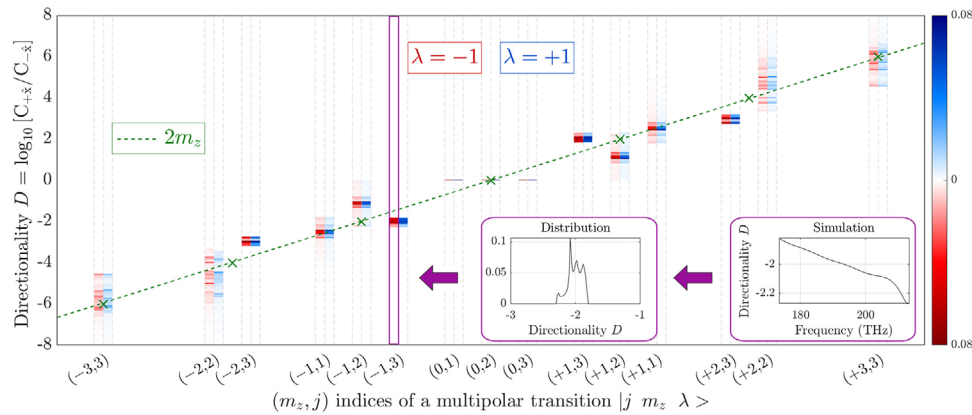


Figure 2. For each (j, m_z, λ) , the graph shows the histogram of the logarithmic directionality of the coupling of the emitter into the waveguide. Each histogram is the distribution of the directionality obtained from a wideband numerical simulation (see inset). A more(less) intense color corresponds to a more(less) frequent occurrence of a particular directionality value in the frequency-dependent simulation results. Blue(red) corresponds to multipolar emissions with positive(negative) helicity. The green dashed line corresponds to $2m_z$: It joins the green crosses whose discrete horizontal coordinates m_z are placed at the mid-point of the (j, m_z) groups. Positive(negative) values of D indicate preferential coupling toward the $+\hat{x}(-\hat{x})$ direction, and $|D|$ measures the degree of directionality in orders of magnitude. The graph shows how D is mostly determined by the eigenvalue of the transverse component of the angular momentum, m_z . The independence of D on the helicity λ is clearly observed.

Figure 3 shows D as a function of frequency for some exemplary cases. All the regularities are clearly visible across the whole spectrum. In particular, we observe in Figure 3a that there is essentially no preferential coupling direction when $m_z = 0$ (note the vertical scale). Half the in-coupled power travels toward each direction. The small fluctuations around $D = 0$ can be attributed to numerical errors. Figure 3b shows that the directionality of all multipolar emissions with $m_z = +1(m_z = -1)$ is positive(negative). In Figure 3b, we clearly observe that the directionality of a particular (m_z, j) emission is opposite to the directionality of the $(-m_z, j)$ emission, and that there is a perfect spectral overlap of the directionality of multipolar emissions with equal (m_z, j) but opposite helicities. The features at ≈ 205.3 THz, also seen in Figure 6, are due to a pronounced dip in the frequency-dependent coupling into the guided mode toward the non-preferred direction.

The exponential dependence of the directionality on the transverse angular momentum is remarkable. Its origin can be traced back to an intrinsic property of the evanescent angular spectrum of the multipolar emissions. Section V, Supporting Information, shows that: i) Only the evanescent plane-waves in the angular spectrum of $|k j m_z \lambda\rangle$ can couple power into the waveguide, and ii) the power flux (real part of the Poynting vector) carried by those evanescent plane-wave components toward the $\pm\hat{x}$ directions is proportional to a term that has a $\pm m_z$ exponential dependence. The origin of the exponential directionality is hence an intrinsic property of the emissions, independent of the details of the waveguide. This generality is consistent with the wide variety of experimental setups where the directional coupling due to transverse angular momentum has been observed.^[1,7,8] The exponential directionality is also in particular consistent with ref. [14], where the transverse angular momentum content of evanescent plane-waves was shown to also depend exponentially on the eigenvalue of transverse angular momentum.^[47] Besides the directionality, the angular momentum of the emissions also affects the coupling efficiency. Figure S2, Supporting Information, shows a rough trend where multipolar transi-

tions with higher multipolar order j and absolute value of the transverse angular momentum $|m_z|$ couple more efficiently to the waveguide, sometimes with a difference of orders of magnitude. This is an important feature, since it can potentially make such multipolar transitions, that are typically relatively weak in comparison to the usual dipolar transitions of the emitters, relevant when it comes to their detection by a waveguiding system. Very similar theoretical predictions regarding the coupling efficiency of higher order transitions have been also reported in ref. [22].

3. Symmetry Analysis

3.1. Transverse Angular Momentum

We now use the invariance of the waveguide upon reflection across the planes yOz (M_x) and xOy (M_z) to infer several fundamental characteristics of the directional coupling effect from the transformation properties of the joint emission-waveguide system. The mirror reflection properties of the helicity ($\Lambda = \mathbf{J} \cdot \mathbf{P}/|\mathbf{P}|$) and angular momentum ($\mathbf{J} = m\mathbf{z}$) of the emissions, and of the power flux toward the $\pm\hat{x}$ directions inside the waveguide ($\mathbf{F} = F\hat{x}$) are hence of relevance. Such transformation properties are readily derived^[48] by noting that the properties of the power flux must be akin to those of linear momentum (\mathbf{P}) and the Poynting vector, and that angular momentum and linear momentum transform differently under parity ($\mathbf{r} \rightarrow -\mathbf{r}$) and mirror symmetries due to their axial and polar vector character, respectively:

$$\begin{aligned} M_x(\mathbf{J}) &= M_x(m\mathbf{z}) = R_x(\pi)[\Pi(m\mathbf{z})] = R_x(\pi)(m\mathbf{z}) \rightarrow -m\mathbf{z} \\ M_z(\mathbf{J}) &= M_z(m\mathbf{z}) = R_z(\pi)[\Pi(m\mathbf{z})] = R_z(\pi)(m\mathbf{z}) \rightarrow m\mathbf{z} \\ M_x(\mathbf{F}) &= M_x(F\hat{x}) = R_x(\pi)[\Pi(F\hat{x})] = R_x(\pi)(-F\hat{x}) \rightarrow -F\hat{x} \\ M_z(\mathbf{F}) &= M_z(F\hat{x}) = R_z(\pi)[\Pi(F\hat{x})] = R_z(\pi)(-F\hat{x}) \rightarrow F\hat{x} \\ M_x(\Lambda) &\rightarrow -\Lambda, \quad M_z(\Lambda) \rightarrow -\Lambda \end{aligned} \quad (3)$$

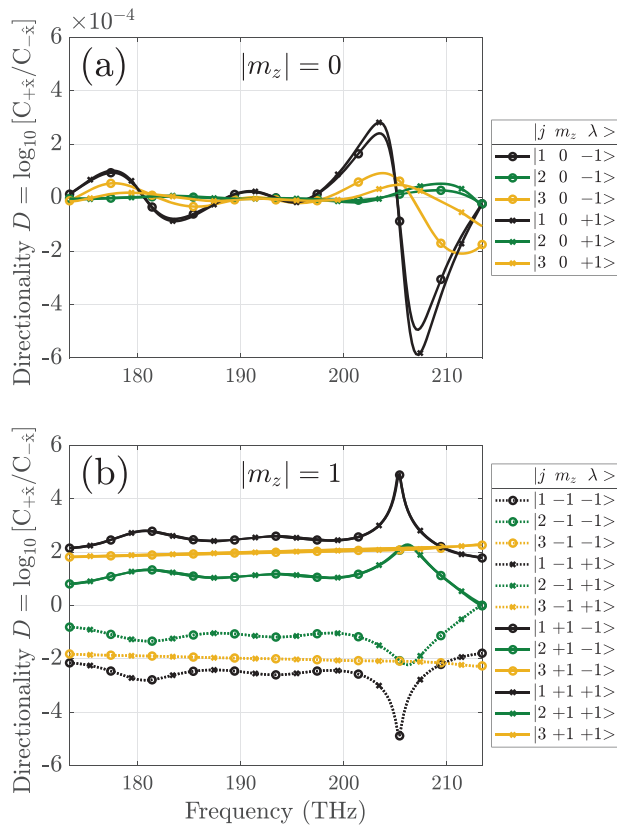


Figure 3. Directionality D with respect to frequency for the coupling of multipolar emissions $|k j m_z \lambda\rangle$ with $j = 1, 2, 3$ and $m_z = 0$ (a), or $|m_z| = 1$ (b). The emitter is located in the xOy plane. Please note the different vertical scales in (a) and (b).

Figure 4 shows the transformations of the initial situations (panels a and e), upon the following symmetries of the waveguide: M_x (panels b and f), M_z (panels c and g), and the composition $M_z M_x$ (panels d and h). Angular momentum is represented by green arrows, positive(negative) helicity by blue(red) circles, and power flux by yellow arrows of different size, reflecting a preferred coupling direction. The angular momentum and helicity of the emission are separately considered in panels (a) to (d), and (e) to (h), respectively. In the initial, yet untransformed, situation of panels (a) and (e), we hypothesize some degree of directional coupling depending solely on angular momentum and solely on helicity, respectively. Such hypothesis is falsified when a transformed system shows a physical contradiction with the original one. For example, the emission in panel (g) occurs from the same location as the emission in panel (e), and, even though the emissions have opposite helicity, they result in the same directionality. Similarly, the emission of panel (h) is from the same location and of the same helicity as in panel (e), but results in the opposite directionality. Such contradictions can only be avoided if the two yellow arrows have identical sizes, that is, if there is no directionality. No such contradictions can be found regarding angular momentum dependent directionality when $|m_z| > 0$. The comparison of panel (a) with panels (b)–(d) only shows that the directionality changes sign with the sign of the transverse

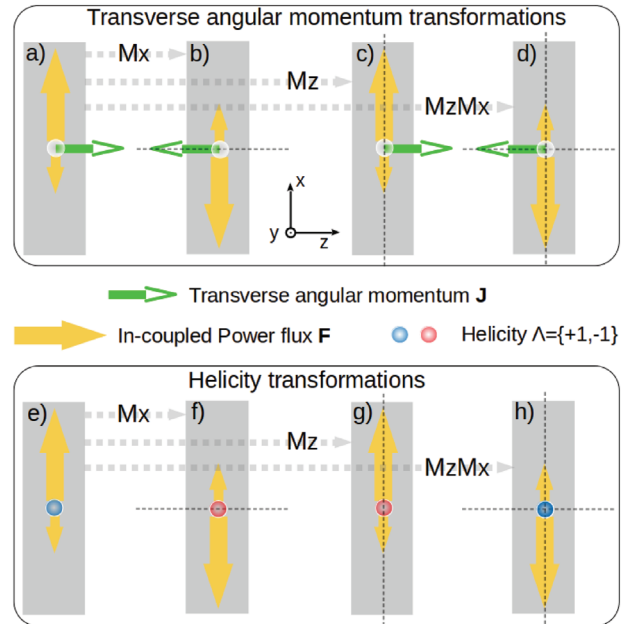


Figure 4. Transformations of transverse angular momentum (green arrows), helicity (red/blue circles), and in-coupled power flux (yellow arrows) upon different reflection symmetries (dashed lines) of the waveguide (gray strips). The initial situations (panels (a) and (e)) are transformed by M_x (panels (b) and (f)), M_z (panels (c) and (g)), and the composition $M_z M_x$ (panels (d) and (h)), respectively. In each panel, the origin of coordinates is at the position of the emitter, and the coordinate axes are oriented as shown in the figure.

angular momentum. The case $m_z = 0$ is special because it is invariant under the action of M_x : $m_z \rightarrow -m_z$ (Equation (3)). This leads to a contradiction between panels (a) and (b), where the same value of $m_z = 0$ would result in opposite directionality. Algebraic derivations can be found in Section IV, Supporting Information, where we show that the M_z symmetry implies that two helical emissions $|k j m_z \lambda\rangle$ and $|k j m_z - \lambda\rangle$ will have the same directionality, and that the $M_z M_x$ symmetry implies that $|k j m_z \lambda\rangle$ and $|k j - m_z \lambda\rangle$ will have opposite directionality. The latter implies $D = 0$ for $m_z = 0$. The simulation results obey all these symmetry-based predictions. The same regularities will occur in any other geometry with the same symmetries. For example: i) the same system as in Figure 1 but with the waveguide turned 90 degrees along its axis; ii) the same system as in Figure 1 or (i) but with a substrate parallel to the xOz plane supporting the waveguide; and iii) a cylindrical waveguide or a tapered fiber.

Let us now analyze the directionality for centered electric and magnetic multipolar emissions with fixed (k, j, m_z) . The facts that the waveguide is symmetric under the M_z mirror symmetry, and that, contrary to the helical emissions, the electric(magnetic) emissions with well-defined transverse angular momentum are eigenstates of M_z , imply the following selection rule (derived in Section IV-A, Supporting Information): A centered electric or magnetic multipolar emission can only couple to a waveguide mode when $\tau q(-1)^{j+m_z} = 1$, where $\tau = +1(-1)$ for electric(magnetic) multipoles and q is the M_z eigenvalue of the waveguide mode. We note that two counter-propagating but

otherwise identical waveguide modes have the same value of q . Therefore, when the selection rule is not met, the emitter cannot couple to any of the two counter-propagating modes, and when the selection rule is met, the emitter can couple to both modes. Numerical simulations (not included) confirm the selection rule. We show in Section IV-A, Supporting Information, that when the coupling is allowed, the directionality for the electric(magnetic) multipoles will be the same as the directionality for the helicity multipoles. In fact, the directionality will be the same for any linear combination of the two helical multipoles $|k j m_z \lambda = \pm\rangle$. In particular, this implies that the directionality of centered electric(magnetic) multipolar emissions will grow exponentially with m_z . Let us illustrate the selection rule using a centered electric dipole emission $|k j = 1 m_z \tau = 1\rangle$ of fixed m_z equal to +1, -1, or 0. The selection rule formula $\tau q(-1)^{j+m_z} = 1$ particularized to $\tau = 1$ and $j = 1$ reads $q(-1)^{m_z} = -1$, which implies that when $q = 1$, the emission will couple into the waveguide if $m_z = +1$ or $m_z = -1$, but not when $m_z = 0$. On the other hand, if $q = -1$, only the $m_z = 0$ case will couple into the waveguide. When the electric dipolar emission couples into the waveguide, its directionality will be exactly equal to the directionality of a dipolar emission with well-defined helicity $|k j = 1 m_z \lambda = \pm\rangle$.

Figure 4 helps elucidating other characteristics of the directional coupling effect. The directionality changes sign upon M_x (panels b and f). This implies the intuitive fact that the emission must break the M_x symmetry to couple directionally. Otherwise, invariance of the emission combined with the change of sign of the directionality would imply $D = 0$. This necessary condition is met by both transverse angular momentum and helicity, which change upon M_x . In light of this, a helicity-dependent directionality may be possible for an emitter displaced out of the xOy plane. The reason is that the displacement breaks the M_z reflection symmetry that forbids helicity-dependent directionality for centered emitters otherwise. This is illustrated in Figure 5: The contradictions between Figure 4e and Figure 4g,h do not occur between Figure 5e and Figure 5g,h because the emitter is not at the original position. Comparison of the top panels of Figures 4 and 5 indicates that the correlation of the sign of the angular momentum with the preferred coupling direction is independent of the displacement. In contrast, the bottom panel of Figure 5 shows that the possible helicity dependent directionality behaves differently: The same helicity can produce opposite directionality depending on the position of the emitter. We confirm the existence of position and helicity dependent directionality for displaced emitters by numerical simulations. Figure 6 shows the directionality of dipolar emissions for an emitter that has been displaced out of the xOy plane by 100 nm along the positive z direction, right to the vertical of the edge of the waveguide, as shown in Figure 5a. Helicity has now some influence on directionality. For example, some directionality can be observed in Figure 6 for $m_z = 0$, in contrast to the centered case in Figure 3a. Also, when $|m_z| = 1$ the curves for $|j = 1 m_z \lambda\rangle$ and $|j = 1 m_z - \lambda\rangle$ are not on top of each other, as is the case for the centered emitter in Figure 3b. Nevertheless, the sign of $m_z = \pm 1$ still determines the sign of D because the influence of helicity in the directionality of a displaced emitter is rather small when compared to the influence of angular-momentum when $|m_z| > 0$. Figure 6 also shows that the coupling direction favored by a given value of helicity changes

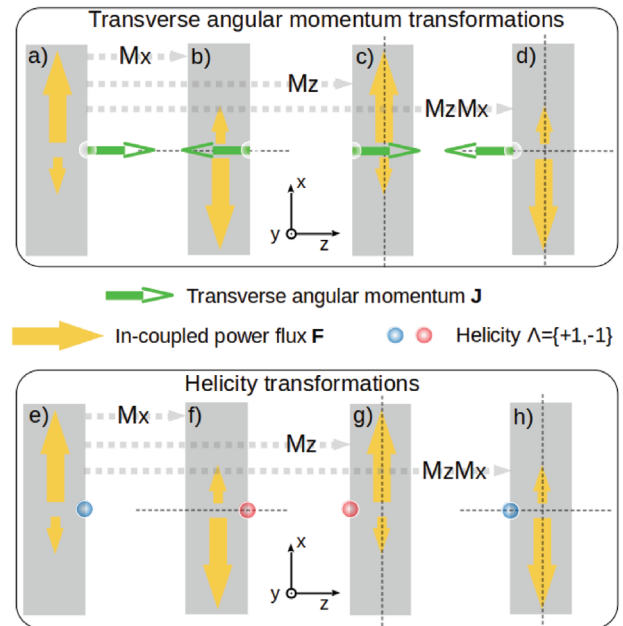


Figure 5. Transformations of transverse angular momentum (green arrows), helicity (red/blue circles), and in-coupled power flux (yellow arrows) upon different reflection symmetries (dashed lines) of the waveguide (gray strips) for an emitter displaced by $d_z = 100$ nm from the xOy plane. In each panel, the origin of coordinates is at the position where the emitter was before the displacement (see Figures 1 and 4) and the coordinate axes are oriented as shown in the figure.

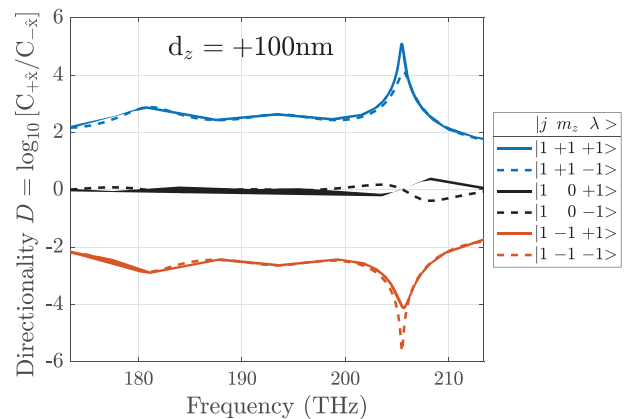


Figure 6. Directionality D with respect to frequency for the coupling of multipolar emissions $|k j m_z \lambda\rangle$ with $j = 1$, $m_z \in \{-1, 0, 1\}$, and $\lambda \in \{-1, 1\}$. The emitter is displaced by $d_z = 100$ nm from the xOy plane, as shown in Figure 5a.

with frequency. The foreseen position independence of the correlation of the preferred coupling direction and the sign of the transverse angular momentum is clear in Figure 6. Finally, we observe that Figure 6 clearly shows the regularity due to the M_x symmetry of the waveguide: Independently of the position of the emitter, two helical emissions $|k j m_z \lambda\rangle$ and $|k j -m_z -\lambda\rangle$ will have the opposite directionality (Section IV, Supporting Information). From now on, we focus on the dominant directionality effect, where the emissions break the M_x symmetry due to the axial

character of the transverse angular momentum (compare panels a and b). The dominant directionality is hence due to an axial vector (transverse angular momentum), not to a pseudo-scalar (helicity). Interestingly, the symmetry breaking by axial vectors has been studied in the context of enantio-selective chemical reactions, where Barron refers to it as “false chirality” (see ref. [49] and the references therein). The correct identification of the origin of the directionality is crucial for understanding that it is not a binary effect: While a pseudo-scalar offers only two possibilities which can explain the sign of D , an axial vector can explain the sign and magnitude gradation of D through the sign and magnitude of the vector, respectively. Since the M_x symmetry is broken by the $mz \rightarrow -mz$ change, the degree of M_x breaking must be related to the magnitude of the change ($|2m|$), which vanishes for $m = 0$, suggesting that D should grow with $|2m|$. As previously discussed, we show in Section V, Supporting Information, that the growth is exponential.

Finally, Figure 4 also allows us to determine whether the directional coupling effect is chiral. Panels (c) and (g) show that the directionality is invariant upon a mirror reflection (M_z) of the emission. The effect has hence a mirror symmetry, which makes it achiral.^[50,51]

3.2. Vertical Angular Momentum

The vertical angular momentum axis, coinciding with our y axis, has been selected in directional coupling experiments like, for example, refs. [2–5, 12]. When a magnetic bias is used for such selection, the signals originating from $m_y = \pm 1$ transitions are distinguished at the detectors because they are produced at different frequencies due to Zeeman splitting.

Importantly, the behavior of the directionality D with respect to the vertical and transverse axis is different. In Figure 7, we use the transformation properties $M_x(m_y y) \rightarrow -m_y y$, and $M_z(m_y y) \rightarrow -m_y y$ to analyze the cases of both centered and displaced emitters. In the top part of the figure, a contradiction between panel (a) and panels (c) and (d) is seen for a centered emitter. Such contradiction does not occur for the displaced emitter in the bottom part of the figure because the emitter is not in the original position. Section IV-B, Supporting Information, contains a proof that, in particular, shows that on a waveguide with both M_z and M_x symmetries the directionality for a centered emitter with well-defined y component of angular momentum will be identically zero. This matches the lack(existence) of directionality for centered(displaced) emitters measured in refs. [3, 5, 12]. Moreover, it also explains the directional coupling of centered emitters when the waveguide itself lacks the M_z reflection symmetry, as in ref. [2]. In such case, the waveguide in panel (a) would be different from those in panels (c) and (d), avoiding the contradiction.

We also deduce from the bottom part of Figure 7 that, in sharp contrast to the m_z case, the sign of the angular momentum dependent directionality is not locked to the sign of m_y . For example, panels (e) and (h) show the same sign of m_y but opposite directionality. This dependence of the preferred coupling direction on the lateral (z) position for fixed m_y has been experimentally observed (^[12], Fig. 3b)). In practice, the z positions of the

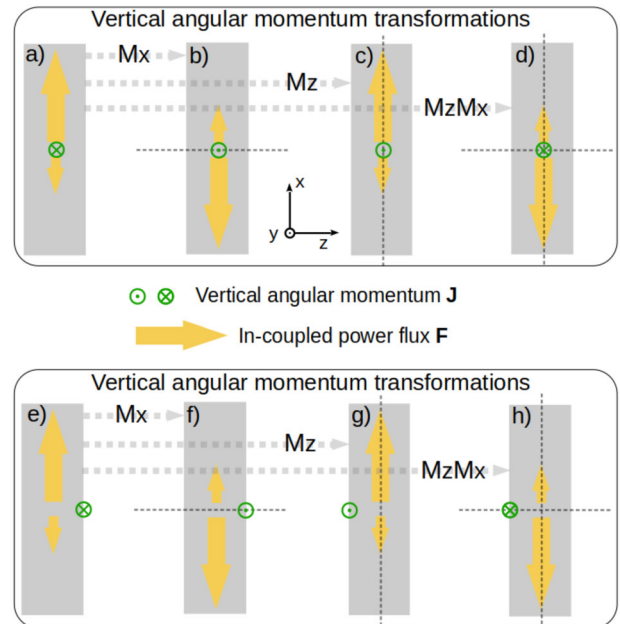


Figure 7. Transformations of the vertical $m_y \hat{y}$ angular momentum (green symbols) and in-coupled power flux (yellow arrows) upon different reflection symmetries (dashed lines) of the waveguide (gray strips). The top(bottom) part shows a centered(displaced) emitter.

quantum dots are often random. Then, the illumination is focused onto a single quantum dot found to be at a particularly favorable position regarding directionality, and such quantum dot is the only contributor to the signals detected at each end of the waveguide. Recently, the controlled positioning of an emitter relative to the waveguide has been achieved using in situ electron beam lithography.^[5] Such technique allows to place a single quantum dot in a favorable location with an uncertainty of some tens of nanometers.

Selecting the vertical axis (y) leads to approximately zero directionality when the positions of the emitters are random and a larger area containing many quantum dots across the whole z -extend of the waveguide is illuminated. The reason is that the sign of the directionality changes when the emitter is on opposite sides of the waveguide (Figure 7). In sharp contrast, if the angular momentum axis is chosen along the transverse direction (z), the preferred coupling direction will be locked to the sign of the angular momentum of the emissions independently of the lateral position of the emitter.^[52] This suggests that changing the magnetic bias direction will potentially have a significant and yet unobserved effect. Let us analyze this possibility, independently of the fact that addressing a single quantum dot may actually be required for some applications.

3.3. Experiment Proposal

We propose an experiment where the quantum dots are embedded inside a host material outside the waveguide, the static magnetic field is applied along the z direction, and instead of addressing a single quantum dot, the pump illuminates a much

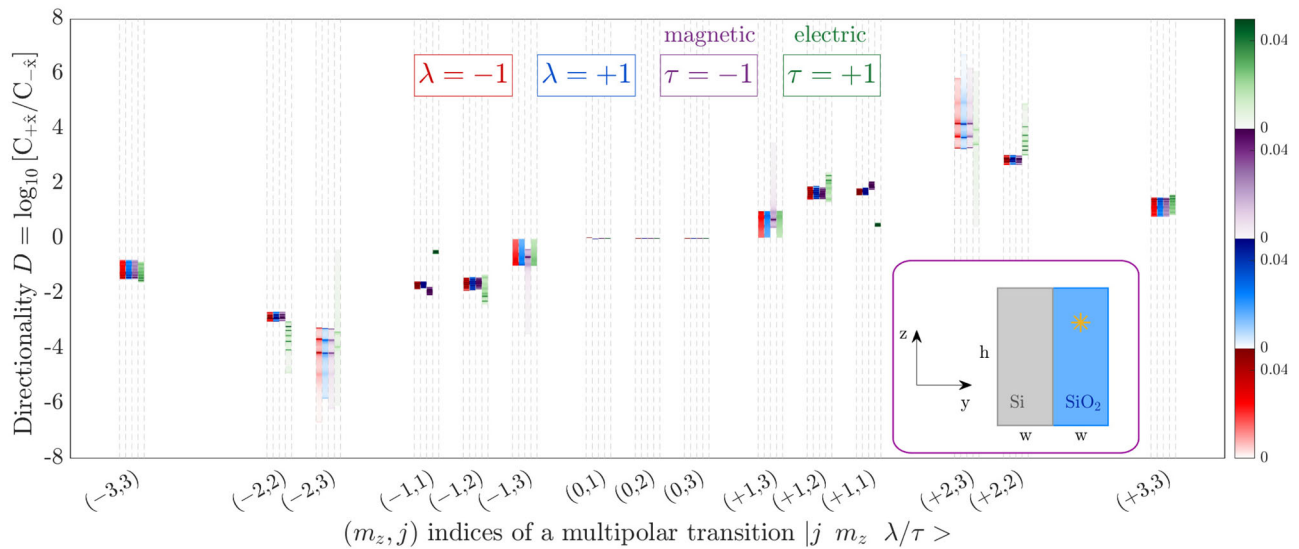


Figure 8. Directionality for helical and electric/magnetic emissions with well-defined angular momentum along the \hat{z} axis for the geometry in the inset, where $w = 200$ nm and $h = 500$ nm. The position of the emitter is marked by the yellow star, placed at the middle of the y extent of the glass slab and at a quarter of its z extent. Figure S3, Supporting Information, shows the coupling efficiencies.

larger area, potentially including many more quantum dots. Previous results in this article indicate that all the $m_z > 0$ emitters will preferentially couple toward one direction and all the $m_z < 0$ emitters will preferentially couple to the opposite one. Therefore, besides showing directionality, the signals at the detectors should be significantly larger than the signals from an individual quantum dot. Assuming incoherent emissions, the total detected average power (photon count) will be larger by a factor equal to the number of quantum dots excited by the pump. Moreover, a super-radiant scaling cannot be ruled out.^[53]

For the proposed experiment, it is important that the quantum dots are not inside the waveguide. Numerical simulations (not included) show that, while the locking of m_z and the sign of the directionality is maintained for dipolar emitters located inside the waveguide and near its top, the directionality decreases significantly with respect to the values in Figure 2. Additionally, the locking is lost in some of the quadrupolar and octupolar emissions. The placement of the emitters near the top of the waveguide is appropriate because symmetry shows that z -biased quantum dots that are embedded exactly in the middle y -coordinate of the waveguide will show zero directionality. We attribute the somewhat different behavior of the emitters inside and outside the waveguide to the fact that the coupling of emitters inside the waveguide is not directly mediated by evanescent fields, which, as we show in Section V-B, Supporting Information, is responsible for such prominent directionality features dependent on the transverse angular momentum of the emission. Therefore, the quantum dots should be embedded in a host material outside the waveguide (see the inset in Figure 8). The refractive index of the host material should be smaller than the effective refractive index of the propagating mode of the waveguide system, to ensure that coupling to the waveguide mode happens predominantly through the evanescent parts of the fields. Accordingly, embedding materials with low refractive index such as glasses and polymers^[54,55] are potentially

more suitable for an experimental realization than embedding materials with high refractive index.^[2–5,56,57]

We now present results from dedicated simulations.

We have used glass, just as an example, as the host material for the numerical simulations presented in Figure 8. The figure shows the directionality of helical and electric/magnetic emitters. The inset shows a cross-section of the considered 3D geometry. The behavior is quite similar for helical and electric/magnetic emitters. For $|m_z| \leq 2$, the directionality exhibits, roughly, a linear dependence on m_z with a slope similar to the slope in Figure 2. The directionality of the $|m_z| = 3$ emissions breaks such linear dependence. We attribute this deviation to the initial multipolar emission reflecting off the air–glass interfaces that gives rise to other multipolar components. Figure S3, Supporting Information, shows the corresponding coupling efficiencies, which, for most cases, grow significantly as $|m_z|$ and j increase. It is worth mentioning that the results in Figures 8 and Figure S3, Supporting Information, correspond to the coupling into a mode that meets the aforementioned condition: Its effective refractive index is larger than the refractive index of glass. The system supports another mode which does not meet such condition, resulting in much reduced directionalities and coupling efficiencies.

We conclude that, excluding the $|m_z| = 3$ emissions, the displaced emitters embedded in glass behave very similarly to the centered emitters in free-space, and should show the aforementioned directionality preserving aggregation of signals from several emitters. We highlight that the aggregation prediction is not limited to the dipolar order. The same proposed experimental setup can be used to test other quantitative and qualitative predictions contained in this article if emitters with $|m_z| > 1$ are available.

For applications that require single quantum dot emission, the combination of the transverse bias direction with the placement of the quantum dot outside the waveguide would relax the

positioning requirements. For example, if the changes that we propose are compatible with controlled positioning techniques, the effects of the remaining position uncertainty would be minimized.

Finally, we note that the angular momentum of the emissions of quantum dots depends on many factors such as the geometry of the dots, their material, the embedding medium, and the magnetic bias direction [158], Chap. 24.1.4]. In particular, the strength of the static magnetic bias needed for achieving a sufficient Zeeman splitting may be different in the transverse and vertical configurations. A detailed study of these points is outside the scope of this article.

3.4. The Huygens' Dipole

In general, the directionality of emissions which contain components with different angular momentum eigenvalues cannot be understood by combining the directionalities of each individual component. In particular, the directionality of an emission is not determined by the average value of angular momentum (unless a single component is present). The interference of the in-coupled fields due to each individual components cannot be ignored. One such example is a Huygens' dipole (see e.g. [19], Fig. 1)), which is a particular combination of an electric and a magnetic dipole. Using our axis, a Huygens' dipole showing directional radiation along $+x$ is obtained by the sum of an electric dipole y plus a magnetic dipole c_0z , where c_0 is the speed of light. With the conventions in Section I, Supporting Information, such Huygens' dipole can be written as the following linear combination of helicity dipoles with well-defined transverse angular momentum $|k j = 1 m_z \lambda\rangle$:

$$\begin{aligned} & -\frac{\sqrt{6\pi\epsilon_0}}{k^3} |\text{Huygens}\rangle \\ &= \frac{i}{2} (|k 1 1 +\rangle - |k 1 1 -\rangle - |k 1 - 1 +\rangle + |k 1 - 1 -\rangle) \\ &+ \frac{1}{\sqrt{2}} (|k 1 0 +\rangle + |k 1 0 -\rangle) \end{aligned} \quad (4)$$

where ϵ_0 is the permittivity of vacuum. The second line of Equation (4) comes from the electric dipole, and the third line from the magnetic dipole. The average transverse angular momentum of the Huygens' dipole is zero. The directionality exhibited by a Huygens' dipole [19] cannot be deduced from the directionalities of its different m_z components in Equation (4), which one could naively combine into an overall directionality equal to zero. Another example is provided by particular linear combinations of two electric dipoles, one with $m_z = +1$ and the other with $m_z = -1$ which, under some conditions, can achieve infinite directionality [8], p. S6, Supp. Inf.].

Importantly, though, the symmetry analysis can still be applied to superpositions of different angular momentum components. For example, it is straightforward to use Equation (S6), Supporting Information, for showing that the Huygens' dipole in Equation (4) is not an eigenstate of M_x because its electric and magnetic parts transform differently (note the sign change in the

third line):

$$\begin{aligned} & -\frac{\sqrt{6\pi\epsilon_0}}{k^3} M_x |\text{Huygens}\rangle \\ &= \frac{i}{2} (|k 1 1 +\rangle - |k 1 1 -\rangle - |k 1 - 1 +\rangle + |k 1 - 1 -\rangle) \\ & - \frac{1}{\sqrt{2}} (|k 1 0 +\rangle + |k 1 0 -\rangle) \neq \alpha \left[-\frac{\sqrt{6\pi\epsilon_0}}{k^3} |\text{Huygens}\rangle \right] \end{aligned} \quad (5)$$

Additionally, Equation (S8), Supporting Information, can be used to show that, if centered, it is an eigenstate of M_z with eigenvalue 1. That is, a Huygens' dipole breaks M_x and, when centered, maintains M_z . Regarding these two symmetries, the situation is the same as in the case of an electric(magnetic) multipolar emission with well-defined m_z . The same situation is achieved by means of two different properties: The axial character of the transverse angular momentum on the one hand, and a particular combination of dipoles on the other. One difference between these two ways is that the breaking of M_x can be increased by increasing $|m_z|$, while the Huygens' dipole does not have a similar quantitative handle.

4. Final Remarks

In this article, we have shown that the analysis of the symmetries and symmetry-breakings of the emitter-waveguide system allows for the unified qualitative understanding of directional coupling in several different situations. We have considered single multipolar emissions with well-defined angular momentum, either centered or displaced from the median plane of the waveguide, and emissions containing different angular momentum components, like the Huygens' dipole. We have shown that, for single multipolar emissions, the directionality is mostly due to the axial character of angular momentum, and that the helicity(handedness) of the emissions plays a much lesser role. We have generalized the spin-momentum locking concept to an exponentially strong locking between the transverse angular momentum and the preferential coupling direction. We have shown that the directionality of the Huygens' dipole arises from the same symmetry and symmetry-breakings as for a single multipolar emission of well-defined transverse angular momentum. We have made several predictions for yet unobserved effects, including a selection rule for the coupling of electric(magnetic) multipolar emissions, and an experiment featuring a transverse magnetic bias for the aggregation of the directional emissions of quantum dots located nearby waveguides.

Regarding other plausible applications of the directional coupling effect: On the one hand, the exponential dependence on transverse angular momentum, and the selection rule for electric and magnetic multipolar emissions, may be exploited for routing, detecting, and classifying the transitions of discrete nano-emitters. On the other hand, contrary to what is sometimes claimed, [6,8] our results indicate that D does not allow to distinguish the helicity, chirality, or handedness of the emission,

and hence the consequently suggested applications for chiral molecule sensing^[59] are not possible. Our framework is particularly suited for understanding and predicting the directional coupling of higher-order multipolar transitions,^[60] which are the object of an increasing number of experimental,^[28–33] and theoretical studies.^[60–64]

Finally, both directionality and coupling efficiency increase significantly with increasing transverse angular momentum. This provides motivation for pursuing the design and fabrication of quantum dots supporting quadrupolar transitions with $|m_z| = 2$, and for selecting the transverse axis instead of the vertical one.

Supporting Information

Supporting Information is available from the Wiley Online Library or from the author.

Acknowledgements

The authors gratefully thank Prof. Heinz Kalt for very useful discussions regarding quantum dots and Dr. Xavier Garcia-Santiago for his insights regarding evanescent coupling efficiencies. The authors warmly thank Ms. Maria Lamprianidou for drawing Figure 1, and Ms. Magda Feló for her help with Figures 4, 5, and 7. The authors acknowledge financial support by the Max Planck School of Photonics, which is supported by BMBF, Max Planck Society, and Fraunhofer Society, and by the Deutsche Forschungsgemeinschaft (DFG, German Research Foundation) under Germany's Excellence Strategy via the Excellence Cluster 3D Matter Made to Order (EXC-2082/1 – 390761711) through its CZF-Focus@HEiKA graduate school. X.Z.-P. acknowledges funding from the European Union's Horizon 2020 research and innovation programme under the Marie Skłodowska-Curie grant agreement No 795838.

Open access funding enabled and organized by Projekt DEAL.

Conflict of Interest

The authors declare no conflict of interest.

Data Availability Statement

The data that support the findings of this study are available from the corresponding author upon reasonable request.

Keywords

angular momentum of light, directional coupling, helicity, symmetry, waveguides

Received: November 17, 2020

Revised: September 3, 2021

Published online:

- [1] R. Mitsch, C. Sayrin, B. Albrecht, P. Schneeweiss, A. Rauschenbeutel, *Nat. Commun.* **2014**, *5*, 5713.
- [2] I. Söllner, S. Mahmoodian, S. L. Hansen, L. Midolo, A. Javadi, G. Kirnsanske, T. Pregnolato, H. El-Ella, E. H. Lee, J. D. Song, S. Stobbe, P. Lodahl, *Nat. Nanotechnol.* **2015**, *10*, 775.

- [3] R. J. Coles, D. M. Price, J. E. Dixon, B. Royall, E. Clarke, P. Kok, M. S. Skolnick, A. M. Fox, M. N. Makhonin, *Nat. Commun.* **2016**, *7*, 11183.
- [4] L. Scarpelli, B. Lang, F. Masia, D. M. Beggs, E. A. Muljarov, A. B. Young, R. Oulton, M. Kamp, S. Höfling, C. Schneider, W. Langbein, *Phys. Rev. B* **2019**, *100*, 035311.
- [5] P. Mrowiński, P. Schnauber, P. Gutsche, A. Kaganskiy, J. Schall, S. Burger, S. Rodt, S. Reitzenstein, *ACS Photonics* **2019**, *6*, 2231.
- [6] L. Fang, H.-Z. Luo, X.-P. Cao, S. Zheng, X.-L. Cai, J. Wang, *Optica* **2019**, *6*, 61.
- [7] J. Petersen, J. Volz, A. Rauschenbeutel, *Science* **2014**, *346*, 67.
- [8] F. J. Rodríguez-Fortuño, I. Barber-Sanz, D. Puerto, A. Griol, A. Martínez, *ACS Photonics* **2014**, *1*, 762.
- [9] F. Le Kien, A. Rauschenbeutel, *Phys. Rev. A* **2014**, *90*, 023805.
- [10] A. Aiello, P. Banzer, M. Neugebauer, G. Leuchs, *Nat. Photon* **2015**, *9*, 789.
- [11] K. Y. Bliokh, D. Smirnova, F. Nori, *Science* **2015**, *348*, 1448.
- [12] B. le Feber, N. Rotenberg, L. Kuipers, *Nat. Commun.* **2015**, *6*, 6695.
- [13] K. Y. Bliokh, F. Rodríguez-Fortuño, F. Nori, A. V. Zayats, *Nat. Photonics* **2015**, *9*, 796.
- [14] I. Fernandez-Corbaton, X. Zambrana-Puyalto, N. Bonod, C. Rockstuhl, *Phys. Rev. A* **2016**, *94*.
- [15] A. Espinosa-Soria, A. Martínez, *IEEE Photonics Technol. Lett.* **2016**, *28*, 1561.
- [16] T. V. Mechelen, Z. Jacob, *Optica* **2016**, *3*, 118.
- [17] P. Lodahl, S. Mahmoodian, S. Stobbe, A. Rauschenbeutel, P. Schneeweiss, J. Volz, H. Pichler, P. Zoller, *Nature* **2017**, *541*, 473 EP.
- [18] M. F. Picardi, A. Manjavacas, A. V. Zayats, F. J. Rodríguez-Fortuño, *Phys. Rev. B* **2017**, *95*, 245416.
- [19] M. F. Picardi, A. V. Zayats, F. J. Rodríguez-Fortuño, *Phys. Rev. Lett.* **2018**, *120*, 117402.
- [20] L. Wei, F. J. Rodríguez-Fortuño, *Phys. Rev. Applied* **2020**, *13*, 014008.
- [21] R. S. Savelev, D. F. Kornovan, V. V. Yaroshenko, M. I. Petrov, *J. Appl. Phys.* **2019**, *125*, 123104.
- [22] J. E. Vázquez-Lozano, A. Martínez, F. J. Rodríguez-Fortuño, *Phys. Rev. Applied* **2019**, *12*, 024065.
- [23] See e.g. the recent special issue^[24] and references therein
- [24] S. M. Barnett, M. Babiker, M. J. Padgett, *Philos. Trans. R. Soc. A: Math., Phys. Eng. Sci.* **2017**, *375*, 20150444.
- [25] A. T. O'Neil, I. MacVicar, L. Allen, M. J. Padgett, *Phys. Rev. Lett.* **2002**, *88*, 053601.
- [26] M. Padgett, R. Bowman, *Nat. Photonics* **2011**, *5*, 343.
- [27] R. P. Cameron, S. M. Barnett, A. M. Yao, *New J. Phys.* **2012**, *14*, 053050.
- [28] S. Tojo, M. Hasuo, T. Fujimoto, *Phys. Rev. Lett.* **2004**, *92*, 053001.
- [29] M. L. Andersen, S. Stobbe, A. S. Sorensen, P. Lodahl, *Nat. Phys.* **2011**, *7*, 215.
- [30] C.-F. Cheng, Y. R. Sun, H. Pan, J. Wang, A.-W. Liu, A. Campargue, S.-M. Hu, *Phys. Rev. A* **2012**, *85*, 024501.
- [31] S. Karaveli, R. Zia, *Opt. Lett.* **2010**, *35*, 3318.
- [32] M. Kasperczyk, S. Person, D. Ananias, L. D. Carlos, L. Novotny, *Phys. Rev. Lett.* **2015**, *114*, 163903.
- [33] A. Vaskin, S. Mashhadi, M. Steinert, K. E. Chong, D. Keene, S. Nanz, A. Abass, E. Rusak, D.-Y. Choi, I. Fernandez-Corbaton, T. Pertsch, C. Rockstuhl, M. A. Noginov, Y. S. Kivshar, D. N. Neshev, N. Noginova, I. Staude, *Nano Lett.* **2019**, *19*, 1015.
- [34] P.-I. Schneider, N. Srocka, S. Rodt, L. Zschiedrich, S. Reitzenstein, S. Burger, *Opt. Express* **2018**, *26*, 8479.
- [35] I. Fernandez-Corbaton, X. Zambrana-Puyalto, G. Molina-Terriza, *Phys. Rev. A* **2012**, *86*, 042103.
- [36] X. Zambrana-Puyalto, X. Vidal, I. Fernandez-Corbaton, G. Molina-Terriza, *Sci. Rep.* **2016**, *6*, 22185.
- [37] X. Zambrana-Puyalto, X. Vidal, P. Wozniak, P. Banzer, G. Molina-Terriza, *ACS Photonics* **2018**, *5*, 2936.

- [38] M. I. Abdelrahman, H. Saleh, I. Fernandez-Corbaton, B. Gralak, J.-M. Geffrin, C. Rockstuhl, *APL Photonics* **2019**, *4*, 020802.
- [39] While angular momentum and helicity can coincide for some particular fields, like circularly polarized Gaussian beams or single plane-waves, this is not true in general. For example, the helicity of vortex beams can be chosen independently from their angular momentum.[36] Angular momentum and helicity are represented by two different commuting operators which generate two distinct symmetry transformations[35, 40]: Angular momentum generates rotations and helicity generates electromagnetic duality,[41, 42] whose action in momentum space is a rotation of the polarization of each plane-wave.
- [40] I. Fernandez-Corbaton, X. Zambrana-Puyalto, N. Tischler, X. Vidal, M. L. Juan, G. Molina-Terriza, *Phys. Rev. Lett.* **2013**, *111*, 060401.
- [41] M. G. Calkin, *Am. J. Phys.* **1965**, *33*, 958.
- [42] D. Zwanziger, *Phys. Rev.* **1968**, *176*, 1489.
- [43] W. Tung, *Group Theory in Physics*, World Scientific, Singapore **1985**.
- [44] A. Lakhtakia, *Beltrami Fields in Chiral Media*, World Scientific, Singapore **1994**.
- [45] The small discrepancies for large $|m_z|$ are due to the low signal to noise ratio of the simulation results in the non-preferred direction.
- [46] The exact slope depends in the particularities of the system, as discussed in Section V, Supporting Information.
- [47] The excitation of a guided mode by an emitting object can be seen as the reciprocal situation of an object being excited by the guided mode. This strongly suggests that the directionality of the evanescent coupling of an emitter into guided modes should also depend exponentially on the transverse angular momentum. We note that, due to a different axis orientation, the y axis is the transverse axis in ref. [14].
- [48] We use the following decomposition of a reflection across a plane perpendicular to a unit vector α : $M_\alpha = R_\alpha(\pi)\Pi$, where Π is the parity transformation ($\mathbf{r} \rightarrow -\mathbf{r}$) and $R_\alpha(\pi)$ a rotation by π along α . Under rotations, angular momentum (\mathbf{J}) and linear momentum (\mathbf{P}) or the Poynting vector transform as vectors, while helicity (Λ) is invariant. Under parity, helicity is a pseudo-scalar which changes sign $\Pi(\Lambda) \rightarrow -\Lambda$, while angular momentum \mathbf{J} and linear momentum \mathbf{P} exhibit the different parity transformation properties of axial and polar vectors, respectively: $\Pi(\mathbf{J}) \rightarrow \mathbf{J}$, versus $\Pi(\mathbf{P}) \rightarrow -\mathbf{P}$.
- [49] L. D. Barron, *Magnetochemistry* **2020**, *6*, 5.
- [50] The definition of chirality is (see e.g., ref. [51, Chap. 2.6]) the lack of parity, all mirror reflections, and all improper rotation symmetries.
- [51] D. Bishop, *Group Theory and Chemistry*, Dover, New York **1993**.
- [52] This statement can be inferred graphically from the top row of Figure 5, and Figure 6 provides a numerical example for it.
- [53] D. F. Kornovan, M. I. Petrov, I. V. Iorsh, *Phys. Rev. B* **2017**, *96*, 115162.
- [54] A. Ekimov, *J. Lumin.* **1996**, *70*, 1.
- [55] T. Trindade, P. O'Brien, N. L. Pickett, *Chem. Mater.* **2001**, *13*, 3843.
- [56] E. Murray, D. J. P. Ellis, T. Meany, F. F. Floether, J. P. Lee, J. P. Griffiths, G. A. C. Jones, I. Farrer, D. A. Ritchie, A. J. Bennett, A. J. Shields, *Appl. Phys. Lett.* **2015**, *107*, 171108.
- [57] P. Schnauber, J. Schall, S. Bounouar, T. Höhne, S.-I. Park, G.-H. Ryu, T. Heindel, S. Burger, J.-D. Song, S. Rodt, S. Reitzenstein, *Nano Lett.* **2018**, *18*, 2336.
- [58] H. Kalt, C. F. Klingshirm, *Semiconductor Optics 1: Linear Optical Properties of Semiconductors*, Springer Nature Switzerland, Cham, Switzerland **2019**.
- [59] P. V. Kapitanova, P. Ginzburg, F. J. Rodríguez-Fortuño, D. S. Filonov, P. M. Voroshilov, P. A. Belov, A. N. Poddubny, Y. S. Kivshar, G. A. Wurtz, A. V. Zayats, *Nat. Commun.* **2014**, *5*, 3226.
- [60] E. Stourm, M. Lepers, J. Robert, S. Chormaic, K. Mølmer, E. Brion, *arXiv preprint arXiv:2002.01278* **2020**.
- [61] J. R. Zurita-Sánchez, L. Novotny, *J. Opt. Soc. Am. B* **2002**, *19*, 1355.
- [62] A. M. Kern, O. J. F. Martin, *Phys. Rev. A* **2012**, *85*, 022501.
- [63] C. M. Dodson, R. Zia, *Phys. Rev. B* **2012**, *86*, 125102.
- [64] A. M. Konzelmann, S. O. Krüger, H. Giessen, *Phys. Rev. B* **2019**, *100*, 115308.